IEEE Access
Multidisciplinary | Rapid Review | Open Access Journal

SPECIAL SECTION ON MULTIMEDIA ANALYSIS FOR INTERNET-OF-THINGS

Received February 13, 2018, accepted March 16, 2018, date of publication April 2, 2018, date of current version April 23, 2018.

Digital Object Identifier 10.1109/ACCESS.2018.2819206

Integrated Dynamics Control System With ESC and RAS for a Distributed Electric Vehicle

XIANYI XIE[1], LISHENG JIN[2], YUYING JIANG[3], AND BAICANG GUO[1]

[1]Department of Vehicle Operation Engineering, Transportation College, Jilin University, Changchun 130022, China
[2]Transportation College, Jilin University, Changchun 130022, China
[3]Department of Ophthalmology, China-Japan Union Hospital, Jilin University, Changchun 130022, China

Corresponding author: YuYing Jiang (jiangyy@jlu.edu.cn)

This work was supported in part by the National Natural Science Foundation under Grant 51575229, in part by the National Key Research and Development Project of China under Grant 2017YFB0102600, and in part by the Electric intelligent Vehicle Innovation Team of the Science and Technology Department of Jilin Province under Grant 20180519022JH.

ABSTRACT An integrated control system developed for improving the vehicle handling and stability under critical lateral motions that includes electric-stability-controller (ESC) and rear-wheel-active-steering (RAS) systems and coordinates the ESC and RAS controllers based on the β-$\dot{\beta}$ phase plane method is discussed in this paper. The ESC includes a fuzzy logical controller that calculates the yaw moment and an additional rear wheel steering angle based on the vehicle steering states. The RAS control system consists of two parts: a feedback controller and a feed-forward controller. When the vehicle in the normal driving situations, the RAS system provides enhanced handling performance. If the vehicle reaches its handling limits, then both ESC and RAS are integrated to ensure vehicle stability. The simulation results demonstrated that the proposed integrated controller system not only can resist external interference and reduce driver fatigue but also improves both vehicle stability and handling.

INDEX TERMS Integrated control, yaw rate, side slip angle, β-$\dot{\beta}$ phase plane, ESC, RAS, stability.

I. INTRODUCTION

In recent years, with improvements in the electric motor and motor controller technology, many possibilities of power train configurations have been proposed [1], [2]. In particular, the distributed electric vehicle has emerged [3].

The greatest distinction between a distributed electric vehicle and a traditional internal combustion engine vehicle is the driving motors are mounted into the wheels, thereby enabling independent control of the motors [4].

An in-wheel motor can be used not only as a driving motor but also as a braking power source, thereby eliminating the need for the traditional complex hydraulic brake system. Electric vehicles with in-wheel motors have many fascinating advantages and provide a new solution for automotive active safety control technology [5], [6].

To date, many automotive active safety technologies have been applied in automobiles, e.g., ESP [7]–[9], 4 WS [8], [9], AFS [7], [9], and ARS [10]–[12].

Along with the development of active steering control technology [7], [8], an increasing number of vehicles are equipped with a rear wheel active steering system (ARS), such as the BMW 7 Series; the ARS can improve the handling stability, while the tire is in the linearity region [9], [10].

The AS (active steer system) control system alters the tire lateral force to control the side slip angle during a steering maneuver, enabling the side slip angle to be nearly zero. Under the nonlinear condition of the tires, AS cannot maintain the driving stability of the vehicle [13]. Because the tire longitudinal force margin is greater than the tire lateral force, once the tire lateral force is saturated, the ability of AS is reduced drastically, and the vehicle may lose its stability [14]. To allow the vehicle to return from the unstable state to the steady state, the ESC, as an active safety technology, is increasingly applied widely in modern vehicles; the ESC achieves yaw moment of the vehicle through differential braking or driving to maintain the stability. However, the frequent intervention of ESC will not only reduce the vehicle speed but also make the driver feel uncomfortable [1]. Therefore, ESC is more suitable for use in nonlinear and extreme conditions.

In summary, a single vehicle dynamics controller cannot balance the driving safety with the handling stability of the vehicles.

However, many researchers have focused on the integration between the active steering system and the braking system [7], [8], [11], [14], and [15]. In reference [14], an

integrated AFS and DYC system was proposed to improve the vehicle stability and handling under various working conditions. The β-$\dot{\beta}$ phase plane was used to determine the stable/unstable region of the vehicle in [8], [9], and [14]. Moreover, activating either AFS, DYC, or both controllers can improve driving safety and handling stability of the vehicle. According to reference [15], the 4 WIS and 4 WID systems can be effectively coordinated to improve the driving safety and handling stability of the vehicle, depending on the relationship of the critical value between yaw rate and vehicle velocity. However, many tests are required to determine the threshold value of the yaw rate and velocity.

A switched model predictive controller [16] and a nonlinear model predictive controller [17], [18] were proposed to coordinate AFS and DYC. An integrated robust model-matching controller was designed using an H∞ technique based on linear matrix inequalities [19]. The proposed controller integrates ARS, longitudinal force compensation and active yaw moment controls. Moreover, in references [20] and [21], a gain-scheduled LPV controller or a control algorithm based on linear parameter-varying (LPV) formulation was used to design the integrated control to coordinate AS and DYC.

However, in the above references, the parameters of the β-$\dot{\beta}$ phase plane do not take the vehicle parameters into account. The effects of individual differences in different control objects are ignored. Although the AFS system can assist inexperienced and nonprofessional drivers, it will lead to intrusiveness in the driver's action [22]. In particular, the corrective steer angle of front wheels by AFS can influence the direction of the vehicle driving.

Thus, the goals of the integrated control system are as follows: (1) to improve the maneuverability and driving stability of the vehicle under various working conditions; (2) to reduce the frequent intervention of ESC and maintain maximum control of the vehicle driving direction for driver. To achieve these goals, this paper presents a proposed integrated control system that includes RAS (represents ''rear wheels active steering'', which different from the ''ARS'' in previous, because the distributed electric vehicle has the function of rear wheels active steering) and ESC controllers. The RAS controller acts as the active steer controller based on LQR theory, and the ESC controller acts as the stability controller, depending on the fuzzy logical response. To take full advantage of these controllers, first, vehicle parameters, side slip angle, vehicle speed and the surface adhesion coefficient of the road-tire are considered to determine the parameters of the β-$\dot{\beta}$ phase plane. Next, this paper attempts to divide the vehicle stable and unstable region based on the β-$\dot{\beta}$ phase law. Finally, the RAS or both RAS and ESC are activated to control the driving safety and handling stability of the vehicle.

The structure of this paper is as follows: In section II, an 8 degree-of-freedom (DOF) vehicle model, including a GIM tire model and a driver model, used in simulation is introduced. In section III, the RAS and ESC controllers are established, and the integrated control strategy of RAS and ESC is presented. The open-loop and closed-loop tests are discussed in section IV. The study's conclusions are presented in section V.

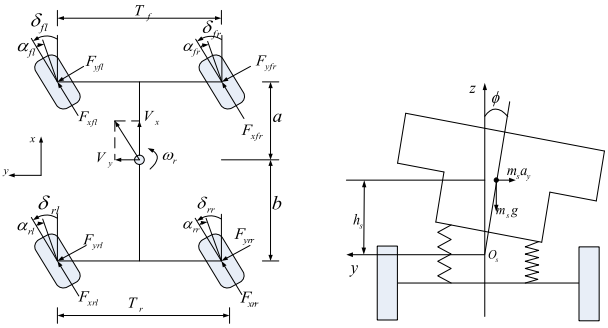

FIGURE 1. Eight degree-of-freedom vehicle dynamics model diagram.

II. SYSTEM MODELING FOR SIMULATION

A. VEHICLE DYNAMICS MODEL

In this paper, the control object is a distributed driving electric vehicle, and the four wheels have the ability to perform driving, braking, and steering independently. To study the dynamic characteristics of the distributed electric vehicle and establish the simulation experiments, the 8 degree-of-freedom vehicle dynamics model with the GIM tire model are established, referencing the methods in [13] and [15], and [13] and [23].

B. DRIVER MODEL

To simulate the behavior of the driver and the driver's characteristics and to perform the closed-loop test, this paper establishes the optimal preview curvature of the driver model [24], [25].

The desired model FWS (front-wheels-steer) angle is calculated by the proposed driver model.

III. DESIGN OF THE RAS AND ESC CONTROLLERS

A. DESIGN OF THE RAS CONTROLLER

As previous discussed, it is well-known that AS (active steer system) has a distinct advantage in the aspects of improving vehicle handling stability.

Generally, the active steering system controller is designed based on the feedback information, including vehicle dynamic parameters, such as the front wheels steering angle, vehicle speed, lateral acceleration, and yaw rate. With the feedback control, the system can effectively reduce the impact of external interference.

In general, the front wheel steering angle is controlled by the driver directly; it is also the primary factor to affect the direction of the driving vehicle. Because the AFS system will lead to intrusiveness in the driver's action [22], to maintain maximum control of the vehicle driving direction for driver, this paper proposes the RAS (rear-wheel active steering) controller [10], [26] to assist the driver to handle the vehicle. The feedback controller is designed based on the optimal control theory of quadratic performance index, minimizing

the tracking errors between the outputs of the actual vehicle model and that of the linear reference model [27].

The linear two-degree-of-freedom vehicle model does not consider the nonlinear characteristics of the tire, nor does it account for the tire side slip characteristics. The linear two-degree-of-freedom vehicle model only considers the vehicle lateral and transverse motion in accord with the Newton's laws of motion.

$$\begin{cases} m \cdot V_x \left(\dot{\beta} + w_r\right) = -\left(k_1 + k_2\right)\beta - \frac{1}{v_x}\left(ak_1 - bk_2\right) w_r \\ \qquad +k_1\delta f + k_2\delta r \\ I_Z \cdot \dot{w}_r = -\left(ak_1 - bk_2\right)\beta - \frac{1}{v_x}\left(a^2k_1 + b^2k_2\right) w_r \\ \qquad +ak_1\delta f - bk_2\delta r \end{cases} \tag{1}$$

where m is the total mass of the vehicle; a and b are the distances from the center of mass to the front and rear axles, respectively; Iz is the vehicle's moment of inertia; $k1$ and $k2$ are the front and rear axle cornering stiffness values, respectively; β is the side slip angle of the vehicle; δf and δr represent the vehicle front and rear steer wheels angle, respectively; Vx and Vy are the vehicle longitudinal speed and lateral speed, respectively. The two degree-of-freedom model is transformed into the equation of state:

$$\begin{aligned} \dot{X} &= AX + BU + CW \\ A &= \begin{bmatrix} -\frac{k_1+k_2}{mV_x} & -\frac{ak_1-bk_2}{mV_x^2} - 1 \\ -\frac{ak_1-bk_2}{I_z} & -\frac{a^2k_1+b^2k_2}{I_Z \cdot V_x} \end{bmatrix}; \\ B &= \begin{bmatrix} \frac{k_2}{mV_x} \\ -\frac{bk_2}{I_Z} \end{bmatrix}; \quad C = \begin{bmatrix} \frac{k_1}{mV_x} \\ \frac{ak_1}{I_Z} \end{bmatrix} \\ \dot{X} &= \begin{bmatrix} \dot{\beta} \\ \dot{W}_r \end{bmatrix}, \quad X = \begin{bmatrix} \beta \\ W_r \end{bmatrix}, \; U = [\delta_r], \; W = \left[\delta_f\right]. \end{aligned} \tag{2}$$

The desired model of the vehicle is as follows:

$$X_d = \begin{bmatrix} \beta_d \\ w_{rd} \end{bmatrix} = A_d\delta_f = A_d W \tag{3}$$

$$\begin{aligned} A_d &= \begin{bmatrix} G_{\beta d} \\ G_{wrd} \end{bmatrix} = \begin{bmatrix} 00 \\ \frac{u}{(a+b)(1+Ku^2)} \end{bmatrix}, \\ K &= \frac{m}{(a+b)}\left[\frac{a}{k_2} - \frac{b}{k_1}\right] \end{aligned} \tag{4}$$

$$e = X - X_d = \begin{bmatrix} e_\beta \\ e_{w_r} \end{bmatrix} = \begin{bmatrix} \beta - \beta_d \\ w_r - w_{rd} \end{bmatrix} \tag{5}$$

where $e(\beta)$ and $e(wr)$denote the side slip angle error and the yaw rate error, respectively; K is the vehicle stability factor, which is the key parameter of the vehicle's stable response character; $G\beta d$ is the ideal model, and the transfer function of any front wheel steer is 0; $Gwrd$ is the steady-state yaw rate gain of front wheel steering vehicle; βd is the ideal side slip angle; Wrd is the ideal yaw rate.

Solving the optimal rear wheels steering angle $U*(t)$ involves minimizing the performance index J:

$$J = \frac{1}{2}\int_0^\infty \left[(X - X_d)^T Q (X - X_d) + U^T R U\right] dt \tag{6}$$

$$Q = \begin{bmatrix} q_\beta & 0 \\ 0 & q_{w_r} \end{bmatrix}, \quad R = [r_r] \tag{7}$$

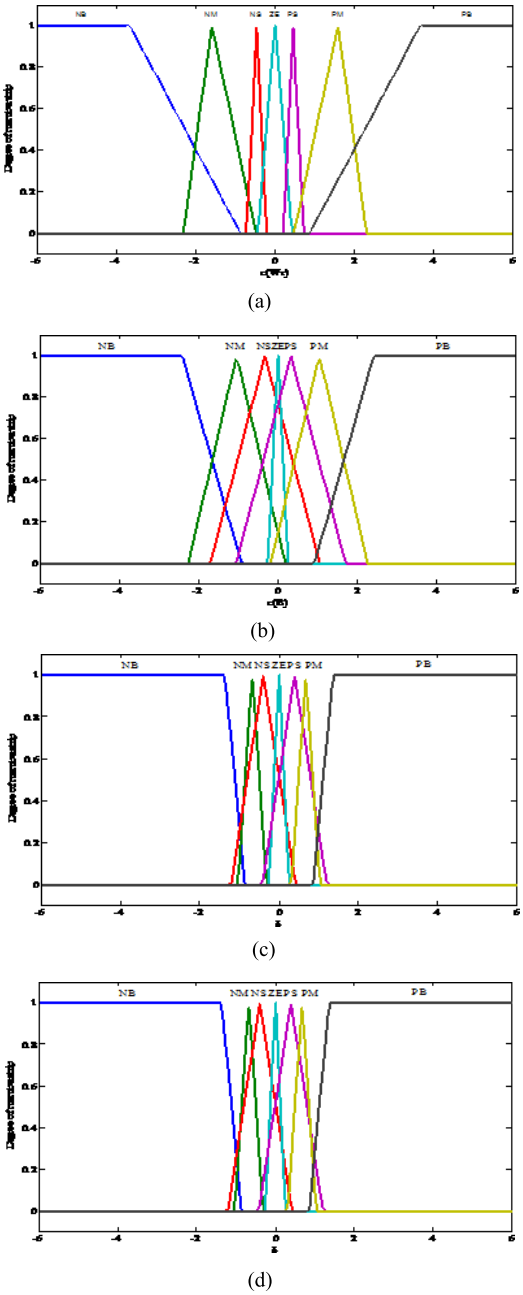

FIGURE 2. Membership function of the fuzzy controller. (a) e(Wr). (b) e(β). (c) Mz. (d) δr.

where Q and R are the weighting matrices of the LQR controller. Q is a semi-definite matrix, and R is a positive definite matrix. The control variables q_β, q_{w_r} and r_r represent the degree of emphasis on the side slip angle β, yaw rate Wr and the rear wheel steering angle δr, respectively. The Hamiltonian function is constructed, and P is the solution of the Riccati equation as follows:

$$Q + A^T + PA - PBR^{-1}B^T P = 0 \tag{8}$$

The solution is given as the final optimal control solution:

$$\begin{aligned} U^*(t) = &-R^{-1}B^T PX \\ &+R^{-1}B^T\left(PBR^{-1}B^T - A^T\right)^{-1}(QA_d - PC)\delta_f \end{aligned} \tag{9}$$

TABLE 1. ESC fuzzy logical rules.

$e(\beta)$ / $e(Wr)$	NB		NM		NS		ZE		PS		PM		PB	
	ΔM	δ_r	ΔM	δ_r	ΔM	δ_r	ΔM	δ_r	ΔM	δ_r	ΔM	δ_r	ΔM	δ_r
NB	PB	PB	PB	PM	PB	PS	PM	ZE	PB	NS	PB	NM	PB	NB
NM	PB	PB	PB	PM	PB	PS	PM	ZE	PB	NS	PB	NM	PB	NB
NS	PS	PM	PS	PB	NS	PM	PS	ZE	PM	ZE	PM	NS	PB	NS
ZE	ZE	PB	ZE	PB	NS	PM	ZE	ZE	PS	NM	ZE	NB	ZE	NB
PS	NB	PS	NM	PS	NM	ZE	NS	ZE	PS	NM	NS	NB	NS	NM
PM	NB	PB	NB	PM	NB	PS	NM	ZE	NB	NS	NB	NM	NB	NB
PB	NB	PB	NB	PM	NB	PS	NM	ZE	NB	NS	NB	NM	NB	NB

The state feedback gain matrix is

$$K_{FB} = -R^{-1}B^T P. \tag{10}$$

Feed-forward gain matrix of front wheel is

$$K_{FF} = R^{-1}B^T \left(PBR^{-1}B^T - A^T\right)^{-1}(QA_d - PC). \tag{11}$$

B. DESIGN OF THE ESC CONTROLLER

In the previous section, the RAS control system was proposed for improving the handling stability of the vehicle by changing the rear wheels steering angle. When the tire is in a non-linear state or the tire force tends to saturate, it is difficult to maintain the stable state by controlling the tire lateral force [9]. Therefore, when the tire is in a non-linear state, the longitudinal force of the tire should be controlled to keep the vehicle in a stable state [9].

The significance of maintaining the stability of the vehicle is no longer to maintain good handling performance but to maintain the response of yaw rate in a reasonable range such that the side slip angle does not exceed the limit.

Under the extreme conditions, controlling the tire longitudinal force can result in correcting the body posture of the vehicle [9],[16]–[18].

According to the authors' previous study results in [13], the ESC controller is designed based on fuzzy logical theory.

Take the deviations between the yaw rate and side slip angle and their own actual values as the inputs of fuzzy controller and the additional yaw moment and the rear wheel angle as the outputs.

Inputs: $e(\beta) = \beta$-βd, $e(Wr) =$ Wr-Wrd;
Outputs: M, δr;
$\{e(\beta), e(Wr)\} = \{$NB,NM,NS,ZE,PS,PM,PB$\}$;
$\{$M, δr $\} = \{$NB,NM, NS,ZE,PS,PM,PB$\}$;

The universe of all variables in the fuzzy controller is set to $[-6, 6]$, according to the actual value, to set $Ke(\beta) = 71$, $Ke(wr) = 51.5$, $KM = 1200$, $K\delta r = 0.0165$. The fuzzy rules of the fuzzy controller are shown in Table 1.

From the previous research results of Reference [13], the membership function of the ESC fuzzy controller is optimized by genetic algorithm; the results are shown as follows:

Compared to controlling a single wheel braking force, adjusting the braking force of the unilateral wheels can maintain a larger longitudinal force margin of the braking wheels. To a certain extent, it is possible to avoid the single wheel tire force saturation. The principle of determining the braking of the wheels is shown in Table 2:

Attach the additional yawing moment from the ESC output to the same side in the form of distribution of braking torque on wheels according to the front and rear load rates on the same side.

For example, when braking the left-side wheels,

$$\Delta M \approx F_{fl} \cdot T_f/2 + F_{rl} \cdot T_r/2 \tag{12}$$

$$F_{fl} + F_{rl} \approx \frac{\Delta M}{(T_f + T_r)/4} \tag{13}$$

$$T_{bfl} = \frac{F_{Z1}}{F_{z1} + F_{z2}} \cdot \frac{\Delta M}{\left(T_f + T_r\right)/4} \cdot r \tag{14}$$

$$T_{brl} = \frac{F_{Z2}}{F_{z1} + F_{z2}} \cdot \frac{\Delta M}{\left(T_f + T_r\right)/4} \cdot r \tag{15}$$

Similarly, the braking force distribution of the right-side wheels can be obtained. *Tbfl* and *Tbrl* are the front and rear wheel braking torque of the left-side wheel, respectively; *Tf* and *Tr* are the wheel distances of the front and rear axles, respectively; and r is the rolling radius of the wheel.

C. INTEGRATED CONTROL STRATEGY OF RAS AND ESC

The RAS system has some advantages in improving the maneuverability of the vehicle, but it has little or no effect on when the lateral tire force is close to the saturation point [15].

ESC has a prominent role in vehicle stability control under extreme operating conditions, but ESC would reduce the vehicle speed. Usually, the driver does not want the ESC system to intervene frequently; thus, the ESC can only play a role in dangerous conditions.

TABLE 2. Principle of selecting braking wheels.

Ideal yaw rate *Wrd*		Error of yaw rate *(Wr-Wrd)*	Steering state characteristics	Braking wheels	Description
Wrd>0 (turn left)	≥0	*Wr*>0, *Wrd*>0; *Wr*>*Wrd*	Oversteer	*W-fr; W-rr*	Define vehicle turning left as the positive direction; setting counterclockwise yaw moment and *δf* is positive
	<0	*Wr*>0, *Wrd*>0; *Wr*<*Wrd*	Understeer	*W-fl, W-rl*	
		Wr<0, *Wrd*>0			
Wrd<0 (turn right)	>0	*Wr*<0, *Wrd*<0; *Wr*>*Wrd*	Understeer	*W-fr; W-rr*	
		Wr>0, *Wrd*<0			
	≤0	*Wr*<0, *Wrd*<0; *Wr*<*Wrd*	Oversteer	*W-fl, W-rl*	

Note: W-fr and W-rr represent the front and rear wheel of the right-side wheels, respectively; W-fl and W-rl represent the front and rear wheel of the left-side wheels, respectively.

As a result, a single chassis control technology cannot meet all the requirements of the vehicle driving in complex and variable conditions. It is necessary to coordinate RAS with ESC and take full advantage of each system. However, because of the existence of dynamic coupling potential conflict between the control targets, the combination of the control systems cannot be completed simply, i.e., a coordinated control method is required.

The phase plane method is one of the common strategies for the analysis of a nonlinear system and the determination of a stable region.

The two types of the vehicle phase plane are the $Wr - \beta$ phase plane stable region and the β-$\dot{\beta}$ phase plane stable region [28]. A related study [2], [28] indicated that the second method is superior to the first; in the strictest sense, side slip angle against yaw rate is not a phase plane plot and therefore physical interpretation of vehicle behavior is difficult. However, the β-$\dot{\beta}$ phase plane can reflect the stability of the vehicle more accurately [28].

Thus, this article refers to the method of determining the $\beta - \dot{\beta}$ phase plane stable region described in [29] and [30]. The $\beta - \dot{\beta}$ phase plane can be affected by velocity of the vehicle and the adhesion coefficient between tire and road surface.

List the state equation of the side slip angle, vehicle speed and the surface adhesion coefficient of the road-tire. Finally, draw the β phase plane expression of the vehicle and use it to judge the vehicle stability state. The parameters of β phase plane expression is $B1 = 0.042$ and $B2 = 0.167$. The concrete expression is as follows:

$$X_{region} = \left|B_1\dot{\beta} + B_2\beta\right| \leq 1. \tag{16}$$

Next, the vehicle β phase plane was divided into ''Stability Region'', ''Instability Region'' and ''Critical Region'', as shown in Fig. 3.

According to the previous discussion, RAS and ESC are different in control mechanism. The ESC is activated to play a role when the vehicle state is lost in the

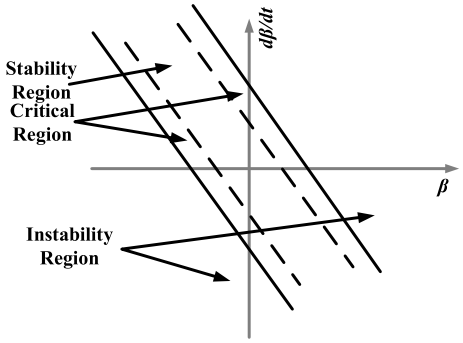

FIGURE 3. Side slip angle phase plane division region.

''Instability Region''; specifically, the β phase plane trajectory curve crosses the outer boundary of the "Critical Region" because the vehicle stability directly depends on the sideslip angle, and the control objective transforms from ascending handling to improve driving stability. ESC provides the extra corrective yaw moment to move the vehicle states back to the stable region through activating the differential braking system, adding an angle to rear wheels to control the side slip angle moreover.

In the ''Stability Region'' of the vehicle β-$\dot{\beta}$ phase plane, improvement of vehicle handling is the main control aim. The RAS system generates the corrective yaw moment to force the yaw rate to follow its desired value through adding a corrective angle to the rear wheels and mining the vehicle sideslip angle by controlling the lateral tire force.

Note that when the vehicle is in the "Critical Region" state, the control objective transforms from ascending handling to improve driving stability. Once the tire lateral force is saturated, the vehicle status will exceed the Critical Region boundary. Because the RAS is no longer able to control the sideslip motion, the ESC is required to control the stability of the vehicle.

To avoid the impact caused by the change of the rear wheel steer angle form δr-RAS to δr-ESC, when the vehicle lost in

TABLE 3. Integrated control strategy

$\beta - \dot{\beta}$ phase plane division region	Xregion	δr	Mz
Stability Region	[0,0.8)	$\delta_{r\text{-}RAS}$	0
Critical Region	[0.8,1)	(5-5Xregion) ·$\delta_{r\text{-}RAS}$	0
Instability Region	[1,+ ∞)	$\delta_{r\text{-}ESC}$	Δ M

Note: δr represents the rear wheel steering angle of the vehicle, $\delta_{r\text{-}RAS}$ represents the rear wheel steering angle of the RAS controller, $\delta_{r\text{-}ESC}$ represents the rear wheel steering angle of the ESC controller, and ΔM represents the additional yaw moment of the ESC controller.

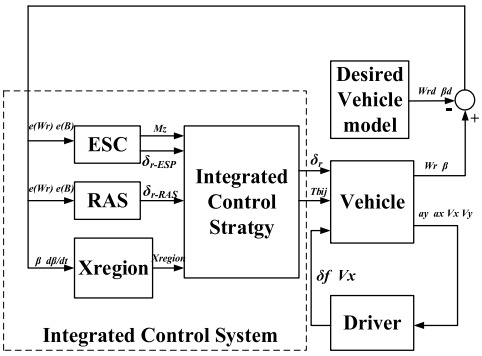

FIGURE 4. Diagram of the integrated control system.

the "Critical Region", the integrated control system sets the corrective rear wheels angle as δr = (5-5Xregion)•δr-RAS to smooth transition, as shown in Table 3 [7].

According to the different areas of the Xregion, the corresponding control strategy is activated to control the vehicle according to the state of vehicle steering. The specific distribution method is shown in the following table:

The diagram of the integrated control system is shown in Fig. 4.

IV. SIMULATION TEST AND ANALYSIS

A. OPEN-LOOP TEST

To analyze the effectiveness of the proposed integrated control system under the open-loop experiment, the initial vehicle speed is set at 80 km/h (approximately 22.22 m/s), and the tire–road adhesion coefficient is set to 0.8[31], [32]. To cause vehicle instability to occur, the sine angle of steering wheel takes a gradual increase in the input, as shown in Fig. 5 (a). In addition, adding FWS and RAS as a comparison, Fig. 5 shows the results of open-loop experiment under the control of the FWS system, RAS control system and the integrated control system.

As shown in Figs. 5(a), (b), and (c), the integrated control system and RAS control system can track the yaw rate well during the simulation time of 0∼6 seconds. With the increase of the steering angle of the front wheels, the yaw rate response of RAS changed dramatically (from 1 to -1.5 rad/s in 0.5 s). The integrated control system can track the yaw rate in a reasonable response depend on the change of δf.

Conversely, the traditional vehicle with the FWS system has a large variation degree, especially the side slip angle. At the time of 2.5 s, the side slip angle of the FWS greatly increases (exceeding 60 deg). The same condition also occurred in the RAS control system at the simulation time of 8 s.

As shown in Figs. 5(e), (f), (h), and (i), the value of the Xregion exceeded 1 at the simulation time periods of t = 2.5 ∼ 3, 3.5 ∼ 4 and 6 ∼ 6.5. The integrated control system provides additional yaw moment to maintain the vehicle posture, which also ensures the stability of vehicles within the periods of 4 ∼ 5.5 and 7.5 ∼ 9, illustrating that the integrated control system distributes the braking force to the unilateral wheels at the previous period stage. As shown in Fig. 5(g), the integrated control system coordinates the RAS and ESC to control the vehicle.

In the remaining time of the simulation time, especially after 6.5 seconds, the value of Xregion does not exceed 1, always remaining below 0.8. The integrated control system no longer attaches the yaw moment to the vehicle, only relying on adjusting the rear wheel steering angle by integrated control system to maintain the handling stability of the vehicle. However, the rear wheel steer angle of the vehicle equipped with RAS system was saturated many times after 6 s.

B. CLOSED-LOOP SIMULATION TEST ON HIGH μ ROAD

In this maneuver, the vehicle moves with desired speed of 120 km/h on a dry road ($\mu = 1.0$). Combining the vehicle model and the driver model, the double-lane-change (DLC) maneuver experiment is performed [33], [34]. The same driver model with FWS is considered for comparison.

Figs. 6(b) and (c) show the vehicle with integrated control system can track the ideal yaw rate well, and the deviation errors of the ideal yaw rate are smaller. However, for the FWS vehicle, the degree of fluctuation of the yaw rate is high, even reaching 0.42 rad/s after 6 seconds of the DLC simulation test. Integrated control system vehicles can maintain a small side slip angle, with the maximum value not exceeding 0.05 rad (close to 2.5). By contrast, the side slip angle of the FWS vehicle fluctuates clearly (even exceeding 5 at approximately 6.5 s, changing from −6 to 5 in 7∼8 s). In Figs. 6(f) and (g), the Xregion value of FWS exceeds 1 during the period of 6∼8 s, and the steer wheel angle changed severely, as shown in Fig. 6(e), causing the FWS vehicle to lose its stability. By contrast, the Xregion of the integrated control vehicle does not exceed 1 during the

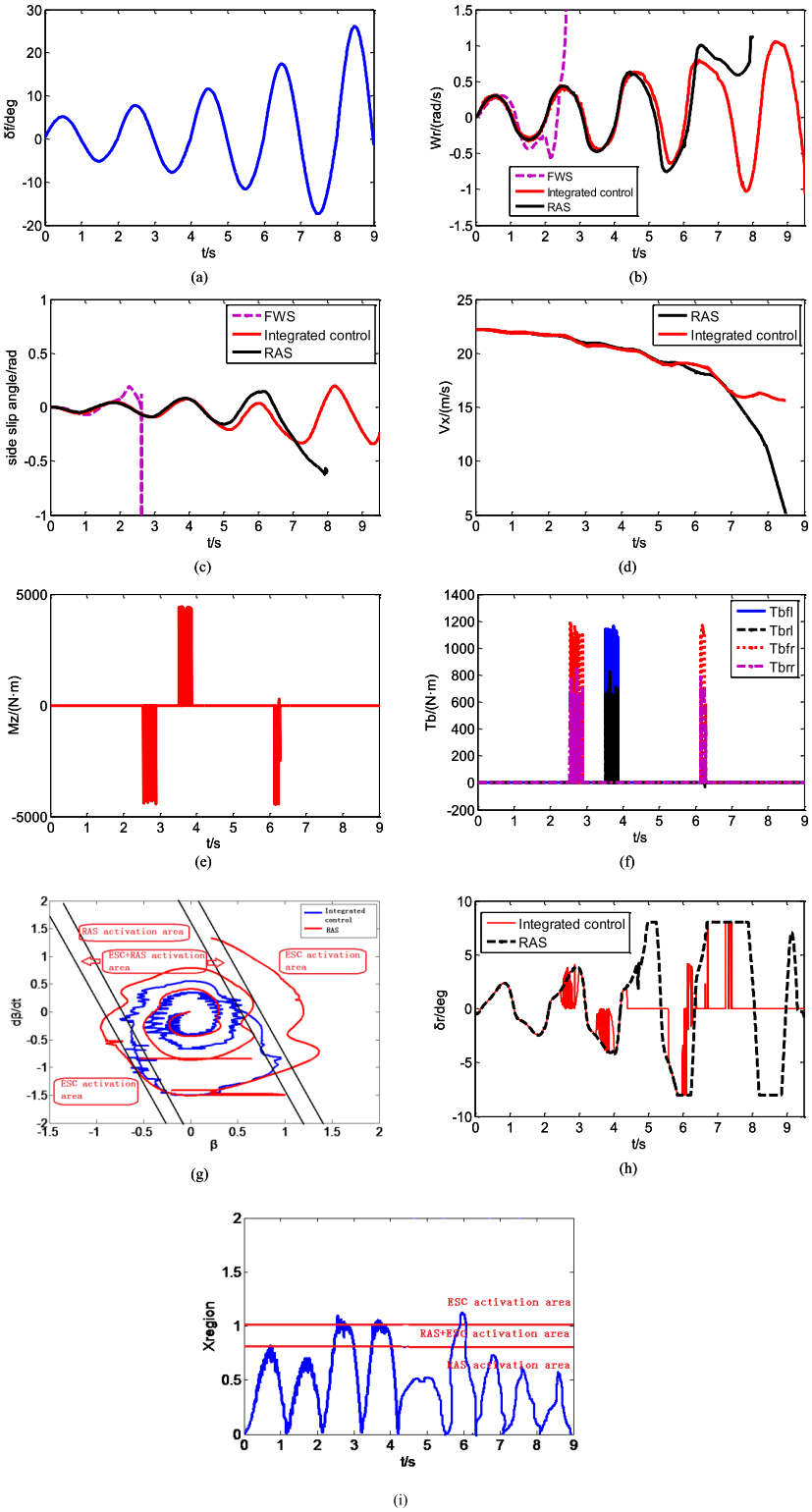

FIGURE 5. Results of the open-loop experiment. (a) front wheels steering angle. (b) yaw rate response. (c) side slip angle response. (d) vehicle speed response. (e) yaw moment by integrated control output. (f) response of braking torque. (g) $\beta - \dot{\beta}$phase plane. (h) rear wheels steering angle δr. (i) Xregion.

simulation. In Fig. 6(h), the δr by integrated control maintained the vehicle driving to be in a stable state. From Fig. 6(a), the travel trajectory of FWS vehicle deviates from the desired path, resulting in an accident at the end of DLC test. From the Vx curve of Fig. 6(d), the integrated control system is found to have a better speed retention ability.

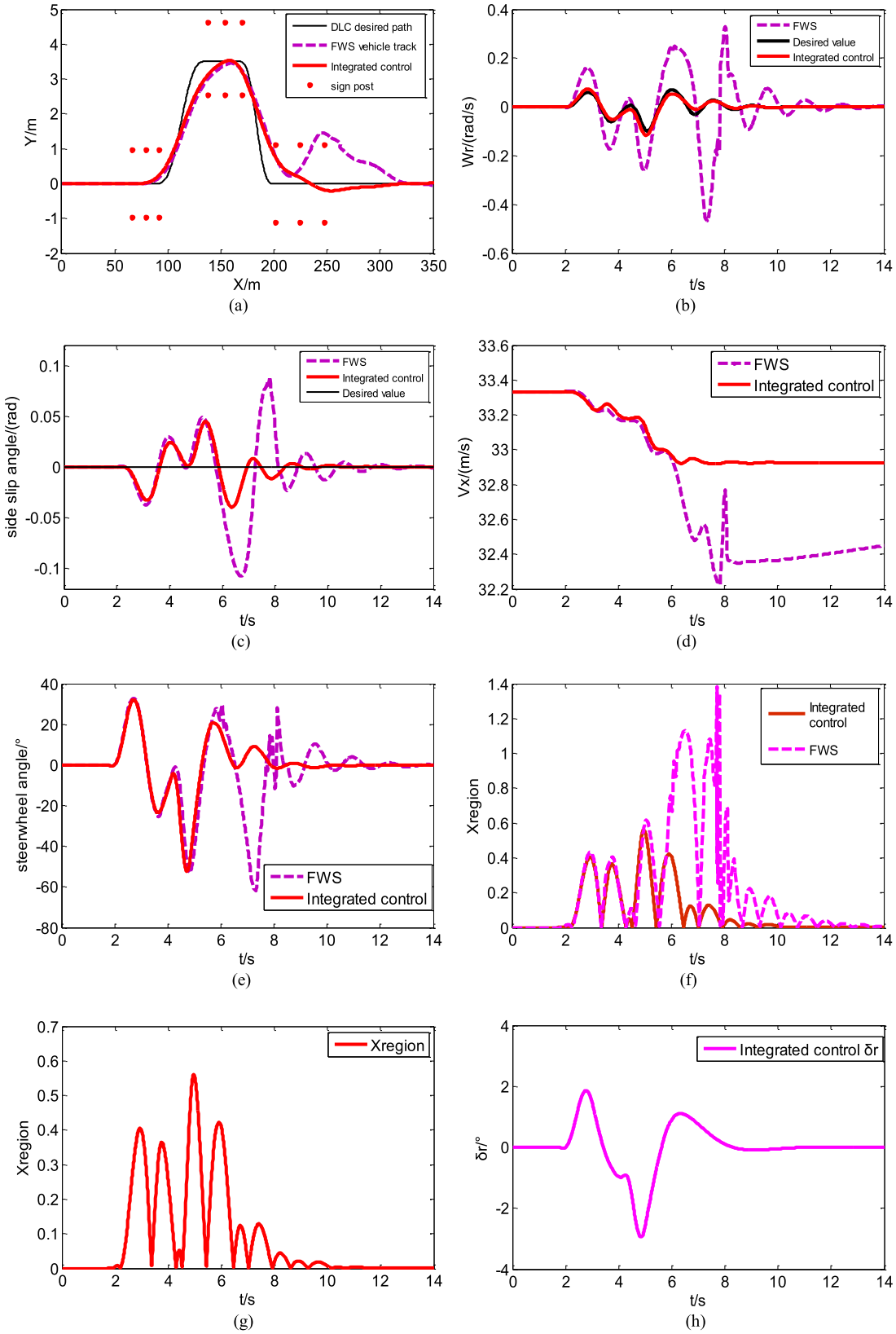

FIGURE 6. Results of the closed-loop experiment on high μ road. (a) Vehicle trajectory of the DLC test. (b) Yaw rate response for DLC. (c) Side slip angle response for DLC. (d) Vehicle speed response for DLC. (e) Response of steering wheel angle. (f) Xregion. (g) Xregion of integrated control. (h) Rear wheels steering angle of integrated control.

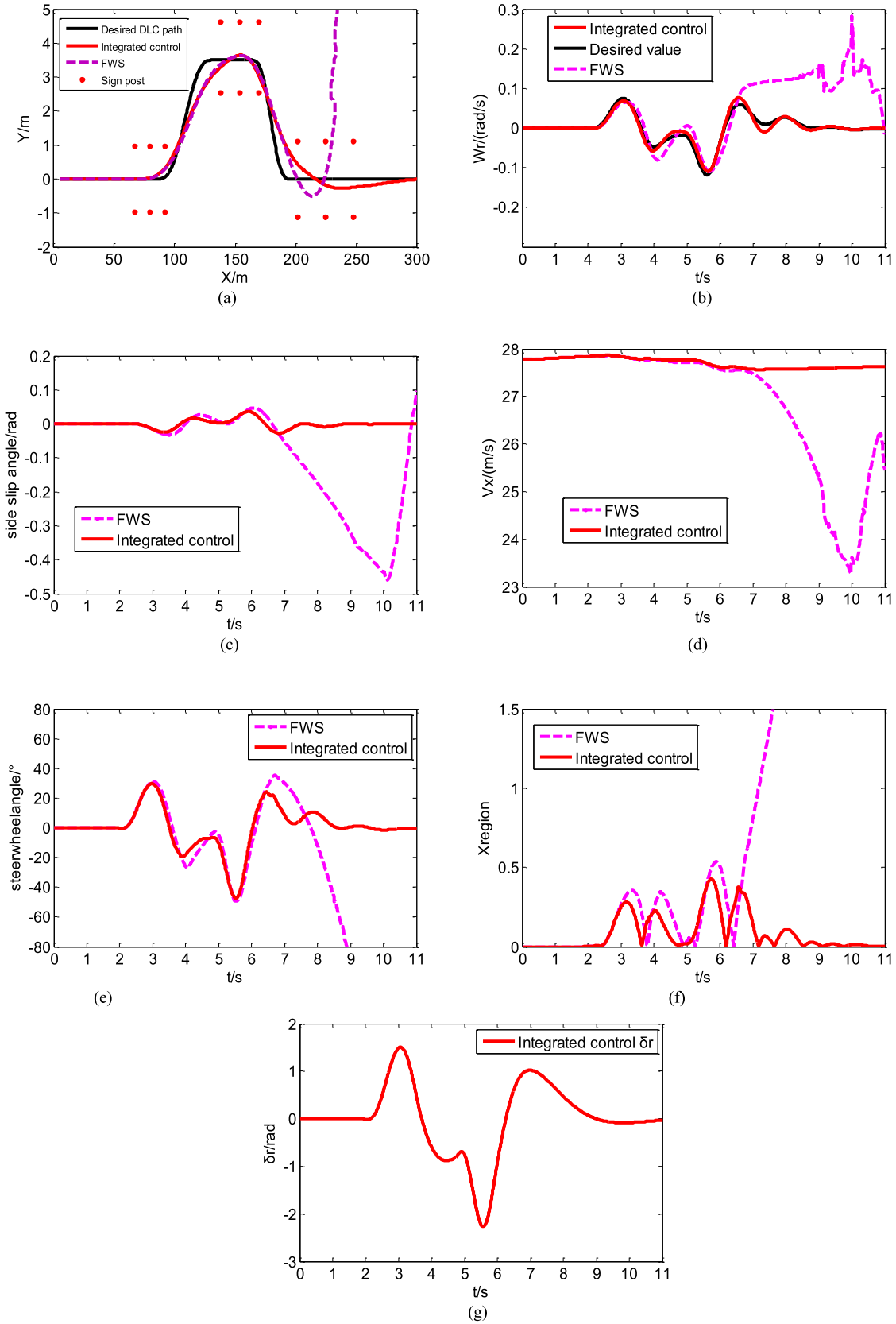

FIGURE 7. Results of the closed-loop experiment on low μ road. (a) Vehicle trajectory of the DLC test. (b) Yaw rate response for DLC. (c) Side slip angle response for DLC. (d) Vehicle speed response for DLC. (e) Response of steering wheel angle. (f) Xregion. (g) Rear wheels steering angle of integrated control.

C. CLOSED-LOOP SIMULATION TEST ON LOW μ ROAD

In this maneuver, the vehicle moves with the desired speed of 100 km/h on a wet road ($\mu = 0.4$) [35]. Comparison of the FWS vehicle with the same driver model is analyzed.

As shown in Fig. 7(b), the vehicle equipped with integrated control system has good yaw rate response ability and can track the desired yaw rate value well, ensuring the Xregion value is no more than 1. The integrated control system successfully played a role in the completion of double-line simulation test. The rear wheels steering angle curve changed smoothly, as shown in Fig. 7(g). At the simulation time from approximately 6.5 to 10 s, the FWS yaw rate response changes severely (more than -0.5 rad/s). The side slip angle decreases sharply (reaching 25) in Fig. 7(c), and velocity of vehicle also decreases sharply in Fig. 7(d). The FWS has deviated from the desired DLC path severely, as shown in Fig. 7(a). From the time of t = 6.5 s, the steering wheel angle continues to increase, indicating that the driver is attempting to correct the body posture of the vehicle, as shown in Fig. 7(e). After 6.5 seconds, from Fig. 7(f), the Xregion curve shows that the Xregion value continues to increase and exceeds 1; as a result, the vehicle with FWS loses its stability.

V. CONCLUSION

The proposed integrated control system consists of an RAS and ESC controller. To organize the integration of RAS and ESC, a β-$\dot{\beta}$ phase plane method based on the vehicle parameters, side slip angle, and yaw rate was employed. To testify the effectiveness of the proposed integrated control system, a number of simulations were performed based on an 8-DOF nonlinear vehicle model in certain critical maneuvers.

The simulation results demonstrated that the integrated control system has better ability to resist external interference in open-loop test. Compared to the vehicle equipped with simple controller, integrated control system enhances the stability of the vehicle significantly.

In a closed-loop test, integrated control system can also help vehicle to complete the DLC test on both high friction coefficient (μ) and low μ roads. The vehicle with integrated control system not only provides good handling and speed retention ability but also reduces the driver's fatigue effectively. The yaw rate response is closer to the ideal value (the error is within 0.15 rad /s), and the magnitude of the side slip angle is small (maximum value is no more than 2.5).

Under this integrated control mechanism, when the vehicle is in the β-$\dot{\beta}$ phase plane stability region, the RAS system is used to enhance the handling stability of the vehicle. When the vehicle is in the β-$\dot{\beta}$ phase plane instability region, both the RAS and ESC systems are used to ensure the driving stability of the vehicle.

In conclusion, the proposed integrated control system is a potential method to effectively control the distributed electric vehicle, greatly improve handling stability, and ensure driving safety.

REFERENCES

[1] J. Chen, "A novel pre-control method of vehicle dynamics stability based on critical stable velocity during transient steering maneuvering," *Chin. J. Mech. Eng.*, vol. 29, no. 3, pp. 475–485, 2016.

[2] S. Inagaki, I. Kushiro, and M. Yamamoto, "Analysis on vehicle stability in critical cornering using phase-plane method," *JSAE Rev.*, vol. 2, no. 16, p. 216, 1995.

[3] X. Cui and G. Chen, "Study on reconfigurable driving force allocation strategy of distributed driving electric vehicle," SAE Tech. Paper 2016-01-8026, 2016.

[4] x. Zhang and D. Göhlich, "Integrated traction control strategy for distributed drive electric vehicles with improvement of economy and longitudinal driving stability," *Energies*, vol. 10, no. 1, p. 126, 2017.

[5] Y. Hori, "Future vehicle driven by electricity and control-research on four-wheel-motored 'UOT Electric March II,'" *IEEE Trans. Ind. Electron.*, vol. 51, no. 5, pp. 954–962, May 2004.

[6] C. Lin and X. Cheng, "A traction control strategy with an efficiency model in a distributed driving electric vehicle," *Sci. World J.*, vol. 2014, Aug. 2014, Art. no. 261085.

[7] J. He, D. A. Crolla, M. C. Levesley, and W. J. Manning, "Coordination of active steering, driveline, and braking for integrated vehicle dynamics control," *Proc. Inst. Mech. Eng., D, J. Automobile Eng.*, vol. 220, no. 10, pp. 1401–1420, 2006.

[8] T. H. S. Li *et al.*, "Design of autonomous and manual driving system for 4 WIS4 WID vehicle," *IEEE Access*, vol. 4, pp. 2256–2271, 2016.

[9] A. Tavasoli, M. Naraghi, and H. Shakeri, "Optimized coordination of brakes and active steering for a 4 WS passenger car," *ISA Trans.*, vol. 51, no. 5, pp. 573–583, 2012.

[10] G. Yin, S. Wang, and X. Jin, "Optimal slip ratio based fuzzy control of acceleration slip regulation for four-wheel independent driving electric vehicles," *Math. Problems Eng.*, vol. 2013, Oct. 2013, Art. no. 410864.

[11] J. Y. Wong, *Theory of Ground Vehicles*, 3rd ed. New York, NY, USA: Wiley, 2001.

[12] J. Zhao, "Chassis integrated control for active suspension, active front steering and direct yaw moment systems using hierarchical strategy," *Veh. Syst. Dyn.*, vol. 55, no. 1, pp. 72–103, 2017.

[13] L. Jin *et al.*, "Study on electronic stability program control strategy based on the fuzzy logical and genetic optimization method," *Adv. Mech. Eng.*, vol. 9, no. 3, pp. 1–13, 2017.

[14] E. Mousavinejad, "Integrated control of ground vehicles dynamics via advanced terminal sliding mode control," *Veh. Syst. Dyn.*, vol. 55, no. 2, pp. 268–294, 2017.

[15] L. Jin *et al.*, "Research on the control and coordination of four-wheel-independent-driving-four-wheel-independent-steering electric vehicle," *Adv. Mech. Eng.*, vol. 9, no. 3, pp. 1–13, 2017.

[16] S. Di Cairano and H. E. Tseng, "Driver-assist steering by active front steering and differential braking: Design, implementation and experimental evaluation of a switched model predictive control approach," in *Proc. 49th IEEE Conf. Decision Control (CDC)*, Dec. 2010, pp. 2886–2891.

[17] P. Falcone *et al.*, "MPC-based yaw and lateral stabilization via active front steering and braking," *Veh. Syst. Dyn.*, vol. 46, no. S1, pp. 611–628, 2008.

[18] J. Tjønnås and T. A. Johansen, "Stabilization of automotive vehicles using active steering and adaptive brake control allocation," *IEEE Trans. Control Syst. Technol.*, vol. 18, no. 3, pp. 545–558, May 2010.

[19] J. Wu *et al.*, "Studies on improving vehicle handling and lane keeping performance of closed-loop driver-vehicle system with integrated chassis control," *Math. Comput. Simul.*, vol. 80, no. 12, pp. 2297–2308, 2010.

[20] M. Doumiati *et al.*, "Integrated vehicle dynamics control via coordination of active front steering and rear braking," *Eur. J. Control*, vol. 19, no. 2, pp. 121–143, 2013.

[21] S. C. Baslamisli, E. Köse, and G. Anlaş, "Gain-scheduled integrated active steering and differential control for vehicle handling improvement," *Veh. Syst. Dyn.*, vol. 47, no. 1, pp. 99–119, 2009.

[22] X. Ma *et al.*, "Multi-objective sliding mode control on vehicle cornering stability with variable gear ratio actuator-based active front steering systems," *Sensors*, vol. 17, no. 1, p. 49, 2016.

[23] G. Gim and P. E. Nikravesh, "An analytical model of pneumatic tyres for vehicle dynamic simulations. Part I: Pure slips," *Int. J. Veh. Design*, vol. 11, no. 6, pp. 589–618, 1990.

[24] Z. Jianling, Y. Zhuoping, Z. Yuancai, and C. Hui, "Driver-vehicle-road closed-loop system modeling method for steering efforts test," in *Proc. IEEE Int. Conf. Veh. Electron. Safety (ICVES)*, Dec. 2006, pp. 228–231.

[25] J. Cao *et al.*, "A driver modeling based on the preview-follower theory and the jerky dynamics," *Math. Problems Eng.*, vol. 2013, Nov. 2013, Art. no. 952106.
[26] G. Chen, X. Gu, and L. He, "An acceleration slip regulation strategy for four-wheel independent drive EV based on road identification," SAE Tech. Paper 2015-01-1106, 2015.
[27] B. Li and F. Yu, "Optimal model following control of four-wheel active steering vehicle," in *Proc. Int. Conf. Inf. Autom. (ICIA)*, Jun. 2009, pp. 881–886.
[28] M. A. Selby, "Intelligent vehicle motion control," Ph.D. dissertation, Dept. Mech. Eng., Univ. Leeds, Leeds, U.K.: 2003.
[29] S. Inagaki, I. Kshiro, and M. Yamamoto, "Analysis on vehicle stability in critical cornering using phase-plane method," *Jsae Rev.*, vol. 2, no. 16, p. 216, 1995.
[30] Y. Yasui, "Improvement of vehicle directional stability for transient steering maneuvers using active brake control," SAE Tech. Paper 960485, 1996.
[31] G. D. Tian, M. C. Zhou, and P. G. Li, "Disassembly sequence planning considering fuzzy component quality and varying operational cost," *IEEE Trans. Autom. Sci. Eng.*, to be published.
[32] G. D. Tian, H. H. Zhang, Y. X. Feng, D. Q. Wang, Y. Peng, and H. F. Jia, "Green decoration materials selection under interior environment characteristics: A grey-correlation based hybrid MCDM method," *Renew. Sustain. Energy Rev.*, vol. 81, pp. 682–692, Jan. 2018.
[33] L. Metz, *Passenger Cars-Test Track for a Severe Lane Change Manoeuvre*, Standard ISO 3888-1, International Standards Organization, 1999.
[34] D. Katzourakis, "Driving simulator parameterization using double-lane change steering metrics as recorded on five modern cars," *Simul. Model. Pract. Theory* vol. 26, pp. 96–112, Aug. 2012.
[35] Z. Wang *et al.*, "Vehicle system state estimation based on adaptive unscented Kalman filtering combing with road classification," *IEEE Access*, vol. 5, pp. 27786–27799, 2017.

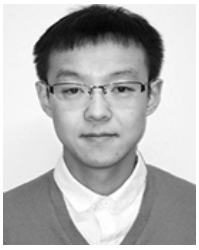

XIANYI XIE received the B.S. degree in vehicle engineering from the Heilongjiang Institute of Technology, Harbin, China, in 2012, and the M.S. degree in vehicle engineering from the Qingdao technology of University, Qingdao, China, in 2015. He is currently pursuing the Ph.D. degree with the Department of Vehicle Operation Engineering, Transportation College, Jilin University, Changchun, China. His research interests include distributed driving/braking/steering electric vehicle active safety, and electric vehicle stability control systems.

LISHENG JIN received the B.S. degree in construction machinery, the M.S. degree in mechanical design and theory, and the Ph.D. degree in mechatronic engineering from Jilin University, Changchun, China, in 1997, 2000, and 2003, respectively. He is currently a Professor with Jilin University. He has published nearly 100 academic papers. His research interests include vehicle safety and intelligent vehicle navigation technology, vehicle ergonomics, and driver behavior analysis.

YUYING JIANG received the B.S. degree in clinical medicine from Jilin University, Changchun, China, in 2002, the M.S. degree from the Department of Ophthalmology, China-Japan Union Hospital, Jilin University, in 2005, and the Ph.D. degree in ophthalmology from the Second Hospital of Jilin University, in 2013. She is currently an Associate Chief Physician with the Department of Ophthalmology, China-Japan Union Hospital, Jilin University. Her research focuses on ocular fundus disease and image processing. She has authored or co-authored over 10 journal and conference proceedings papers in the above research areas.

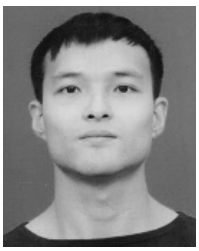

BAICANG GUO received the B.S. degree in vehicle engineering from Northeast Forestry University, Harbin, China, in 2014, and the M.S. degree from Jilin University, Changchun, China, in 2018. He is currently pursuing the Ph.D. degree with the Department of Vehicle Operation Engineering, Transportation College, Jilin University. His research interests include secondary task driving, machine learning, and deep learning.